Effective Viscosities in Thin Ionic Micellar Liquid Films

Maria L. Pollard and C. J. Radke
Dept. of Chemical Engineering and Earth Sciences Div., Lawrence Berkeley Laboratory, University of California, Berkeley, CA 94720

Thin liquid films stabilized by surfactants above the critical micelle concentration exhibit stratification or stepwise dynamic thinning. A continuum hydrodynamic model is outlined for stepwise film thinning that incorporates equilibrium micellar structuring through self-consistent oscillatory disjoining pressures and effective viscosities. Effective viscosities as functions of thickness are evaluated with an extension of the local average density model, considering dilute colloidal suspension shear viscosities and solvent effects. To establish local shear viscosities, structured DFT micellar profiles, coarse-grained densities, and disjoining pressure are used. Ionic micelles and other colloidal systems with repulsive interactions show structured effective viscosities that are generally less than the corresponding homogeneous solution shear viscosity, bounded by the pure solvent viscosity and that of the bulk micellar solution. For 0.1 and 0.2-M sodium dodecylsulfate micellar solutions, the effective viscosities are less than 5 and 10%, respectively, below the homogeneous fluid viscosity, except at small thicknesses, indicating that the micellar film thins faster than a pure water film of the same thickness.

Calculated thinning curves closely resemble experimental observations in the stepwise thinning behavior, displaying decreasing slopes and increased step durations at later times. Despite the micellar structuring within the film, the ionic micelles do not contribute appreciably to the viscous resistance of the thinning film. Rather, Reynolds' film thinning is obeyed, with the equilibrium oscillatory disjoining pressures driving the stepwise dynamics. The shear viscosity of the ionic micellar film is well approximated by that of the bulk solution.

Introduction

The static and dynamic behavior of confined charged colloidal fluids has received considerable attention of late. These fluids exhibit ordering characteristics, both in bulk and in confined geometries, similar to hard sphere fluids, but at very dilute concentrations and over significantly larger length scales due to long-range electrostatic interparticle forces. Very recently equilibrium measurements have appeared for disjoining pressures or interaction forces in foam and pseudoemulsion films of aqueous, ionic micellar solutions (i.e., surfactant solutions above the critical micelle concentration) (Bergeron and Radke, 1992; Bergeron, 1993; Bergeron and Radke, 1995), and for interaction potential energies in ionic micellar films confined by solid-supported bilayers (Richetti and Kékicheff, 1992). The measured forces between the interfaces as a function of separation distance are oscillatory with the degree of oscillation depending on the bulk colloid volume fraction and electrolyte concentration.

In analogous dynamic experiments (Nikolov and Wasan, 1989; Nikolov et al., 1990; Bergeron et al., 1992; Bergeron and Radke, 1992; Sonin and Langevin, 1993; Bergeron and Radke, 1995; Krichevksy and Stavans, 1995), micellar films show pronounced stepwise thinning or stratification, where the step size is comparable with the characteristic distance of the equilibrium-force oscillations. Visual inspection of single horizontal and vertical films at surfactant (and salt) concentrations above the critical micelle concentration (CMC) shows that as the films thin beyond the range of interference colors

Correspondence concerning this article should be addressed to C. J. Radke.
Present address of M. L. Pollard: Department of Chemical Engineering, City College of New York, 140th St. and Convent Ave., New York, NY 10031.

(below ~ 500 nm), progressively darker spots (lighter spots in pseudoemulsion films) of reduced thickness form in the film and expand to engulf it, as has been observed since the work of Johonott (1899) and Perrin (1918) at the turn of the century. The stratification of the film is further evidenced by nonmonotonic, discrete changes in the film thickness during thinning. At each step of the thinning, expulsion of a fluid layer is initiated by the formation and subsequent expansion or sheeting of a "hole," a reduced thickness region in the film (Bergeron and Radke, 1992; Sonin and Langevin, 1993). Hole-sheeting and stratification models have to date approximated the micellar film viscosity with that of the aqueous solution.

Nikolov and coworkers (1989, 1990) were the first to study extensively stepwise thinning in micellar films. They observed the number of steps to increase and the step distance to decrease at higher surfactant concentrations. Added electrolyte substantially suppressed the stepwise thinning behavior. Longer chain length surfactants resulted in more steps for the same amphiphile concentration, with little change in the stepsize. Stratification was also observed in foam films of latex and silica particles (Nikolov and Wasan, 1989; Nikolov and Wasan, 1992; Wasan et al., 1992).

Figure 1 displays data of Bergeron and Radke (1992) for the stepwise thinning of a 0.1-M sodium dodecylsulfate (SDS) foam film in a modified Mysels-Exerowa cell (Mysels and Jones, 1966; Exerowa et al., 1987) at constant capillary-suction pressure. The capillary pressure, P_c, the difference between the bulk external (gas) and internal (liquid) pressures, acts to thin the film, whereas the repulsive disjoining pressure, Π, acts to stabilize the film. Transient film thicknesses are recorded interferometrically by continuously monitoring the intensity of reflected monochromatic light. As the film thins, pronounced steps are seen. Slopes of the ledges between the steps decrease, and their extents increase in time. Finally, a metastable equilibrium thickness is achieved at approximately 25 nm in Figure 1 where the disjoining and capillary pressures balance, at 65 Pa.

Bergeron and Radke (1992) established that the equilibrium disjoining pressure isotherm for 0.1-M SDS is oscillatory for film thicknesses less than 50 nm, with increasingly larger force oscillations as the film thickness is reduced. They offer an explanation of the observed nonmonotonic thinning kinetics in terms of the classic Stefan–Reynolds drainage equation for circular, plane-parallel films (Stefan, 1874; Reynolds, 1886):

$$\frac{dh}{dt} = -\frac{2h^3}{3\pi R^2}\frac{[P_c - \Pi(h)]}{\eta}, \tag{1}$$

where h and R are the film thickness and radius, respectively, t is time, and η is the Newtonian viscosity of the liquid. As the film thins along a repulsive branch ($\Pi > 0$) to a local maximum of the disjoining pressure isotherm, the driving force for thinning, $P_c - \Pi$, diminishes. This causes the slow rates of drainage along the step intervals in Figure 1. Further thinning beyond the local disjoining pressure maximum exposes the film to a region of the disjoining pressure isotherm of positive slope. Such regions in which $d\Pi/dh > 0$ are well known to be thermodynamically unstable (Vrij, 1966). Hence, the film suffers an instability, coined "hole-sheeting" (Bergeron et al., 1992), and thins catastrophically to the next stable branch of the disjoining pressure isotherm where, again, $P_c - \Pi$ diminishes and another step plateau, of longer duration, appears in the thinning curve. Eventually, a large enough stable branch of the disjoining pressure isotherm balances the capillary suction pressure, as in the figure, or the film ruptures. Bergeron and Radke (1992) quantitatively reproduce the thinning dynamics in Figure 1 using the measured disjoining pressures and Eq. 1 with the film viscosity taken as that of the bulk micellar solution in the film Plateau border. Likewise, Bergeron et al. (1992) successfully model the hole-sheeting instability, including the experimentally observed rim circumscribing the expanding hole, using the homogeneous bulk viscosity of the micellar solution. Nevertheless, the measured oscillatory disjoining pressures argue for significant equilibrium structuring of surfactant aggregates within micellar films. Thus, it is not clear that a bulk shear viscosity is appropriate for micellar films undergoing stratified drainage. Here we present a self-consistent calculation of the effective viscosity of such thinning micellar films.

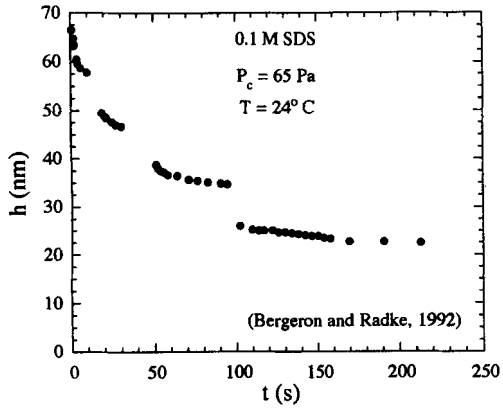

Figure 1. Dynamic thinning of an 0.1-M SDS foam film, Bergeron et al. (1992).

The slopes of the four step intervals (regions with data points) decrease at later times. Likewise step intervals increase in duration as thinning progresses.

Recently, we proposed a density functional model (Laso, 1993; Pollard and Radke, 1994) to predict oscillatory disjoining pressures from calculated equilibrium inhomogeneous micelle distributions in thin liquid films. The model treats the micelles as large macromolecules that pack and order between rigid film interfaces in much the same manner as confined molecular fluids. Given specific forms for the isotropic micelle interparticle potentials and the external field from the charged film interfaces, the resulting calculated micelle density profiles and corresponding disjoining pressures are oscillatory, with the micelle–micelle electrostatic interactions determining the magnitude and distance scaling of the oscillations. Comparison to the experiments of Bergeron and Radke (1992) and Bergeron (1993) demonstrates that the model indeed captures all the qualitative features of the data, including the effects of varying surfactant type and concentration, and added salt. In this article, we incorporate these inhomogeneous micellar profiles into a self-consistent continuum hydrodynamic framework and thereby evaluate effective viscosities for draining micellar films.

To evaluate the micellar film effective viscosity we extend the local average density model (LADM) of Bitsanis et al. (1987, 1988) for confined molecular fluids. LADM applied to colloid films establishes the local shear viscosity of the micellar suspension in the film that is subsequently inserted into the squeeze-flow hydrodynamic equations for film thinning. Combining these two descriptions reveals the effective viscosity as a function of film thickness.

Density-Functional Micellar Film Model

The fluid between the liquid film interfaces is composed of spherical monodisperse charged micelles of diameter d in a background dielectric continuum of water, surfactant monomer at the CMC, and dissociated counterions from micelles and monomers, as depicted in Figure 2. We consider inhomogeneities only in the x-direction, normal to the film interfaces; the fluid is treated as isotropic over planes parallel to the interfaces. Micelles interact via radially symmetric pair potentials, screened by the other ions, and are in chemical equilibrium with micelles in the contiguous bulk solution. We represent the adsorbed layer of surfactant at each interface as a rigid, uniformly charged wall of a prescribed surface charge density. The micelle–wall interaction is of a colloidal sphere–plate type, also screened by the electrolyte background.

Our density-functional theory (DFT) relies on expressing the grand potential of the film as a functional of the micelle distribution through the film. Equilibrium requires the grand potential to be minimized, yielding the governing equation for the micelle profile through a film of thickness h (Pollard and Radke, 1994);

$$\mu(\rho^0_{\text{mic,N}}) = kT \ln \rho_{\text{mic,N}}(x) + \int_0^h \rho_{\text{mic,N}}(x_1) \frac{\delta f_0}{\delta \rho_{\text{mic,N}}(x)} (\overline{\rho_{\text{mic,N}}}(x_1)) dx_1 + \int_0^h \rho_{\text{mic,N}}(x_1) U^{\text{eff}}_{\text{mic-mic},x}(|x - x_1|) dx_1 + U^{\text{ext}}(x;h). \quad (2)$$

Here $\rho_{\text{mic,N}}(x)$ is the number density of micelles at position x normal to the film interfaces located at $x = 0$ and $x = h$. To evaluate the micellar disjoining pressure and the film effective viscosity we seek this distribution function. Also, μ is the uniform chemical potential of micelles relative to the standard state, f_0 is the local hard sphere excess free energy, k is Boltzmann's constant, T is temperature, and $\rho^0_{\text{mic,N}}$ is the bulk number density of micelles in the contiguous solution, with which the micelles in the film are in equilibrium. The main inputs to the model are the micelle pair potential $U^{\text{eff}}_{\text{mic-mic},x}$ and the micelle-interface external potential U^{ext}. Smoothed number densities $\overline{\rho_{mic,N}}(x)$ are calculated with the nonlocal Tarazona model (Tarazona, 1985), shown previously to be accurate for hard sphere and Lennard–Jones fluids (Vanderlick et al., 1989).

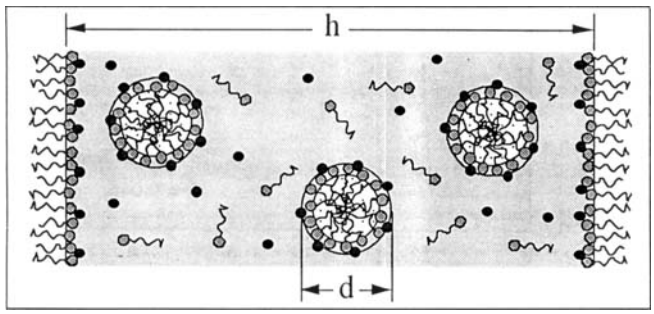

Figure 2. Micellar film section.

The model represents the film interfaces as charged walls separated by distance h, the micelles as charged spheres of diameter d, and dissociated ions as a screening electrolyte continuum background.

The disjoining pressure, Π (Derjaguin and Landau, 1941), is the total excess normal stress in a film, describing the net interaction between the film interfaces through the intervening fluid. The disjoining pressure corresponding to the micelle distributions is expressed as

$$\Pi(h) = \Pi_{\text{DLVO}}(h) - \int_0^h \rho_{\text{mic,N}}(x) \frac{dU^{\text{ext}}}{dx}(x;h) dx - P_{\text{micbulk}}, \quad (3)$$

where the first term on the right side is the classic, continuum, wall–wall DLVO interaction (Derjaguin and Landau, 1941; Overbeek, 1952), comprised of the sum of electrostatic repulsion and van der Waals attraction between the interfaces. The second and third terms represent the osmotic micelle contribution to the disjoining pressure Π_{mic}. Since stratification typically occurs beyond the thickness range of Π_{DLVO}, we only consider Π_{mic} in what follows. P_{micbulk} is the osmotic pressure of the micelles in the contiguous bulk solution of the film plateau border. Details on the approximations involved in these equations and solution methods are provided elsewhere (Laso, 1993).

Resulting density profiles show structuring of the micelles into diffuse layers whose separation is characterized by the decay length of the potentials. This characteristic length is the micelle diameter d plus its Debye atmosphere $2(1/\kappa)$, κ being the inverse Debye length. A typical calculated micelle profile through a symmetric foam film of thickness $h/d = 10$ is displayed in Figure 3, showing five micellar layers. The micelle pair potential parameters are chosen to represent a 0.1-M SDS solution without added salt; screened-Coulomb Yukawa-type potentials were used to generate the profile. A moderately low charge density of $\sigma_{\text{int}} = -0.5\ \mu\text{C/cm}^2$ scales the external potential experienced by the micelles from the interfaces. For this SDS concentration, the bulk micelle number density is $0.0874/d^3$ corresponding to a volume fraction of $\Phi = 4.6\%$, given by the solid line in Figure 3. The Tarazona smoothed density for the evaluation of the excess free energy is shown by the dotted line in Figure 3.

Although the micelles form layers whose density can exceed twice the corresponding bulk density, shown as a solid horizontal line in Figure 3, the electrostatic repulsion between the micelles and between the micelles and the interfaces causes the average micelle density in the film to fall below that in the bulk. The average micelle number density, $\langle \rho_{\text{mic,N}}(x;h) \rangle$, as a function of film thickness is depicted in Figure 4. Note that $\langle \rho_{\text{mic,N}}(x;h) \rangle$ exhibits a general decreasing trend, as the thickness is reduced until at $h/d \sim 2$ all the micelles are expelled from the film. This behavior is typical

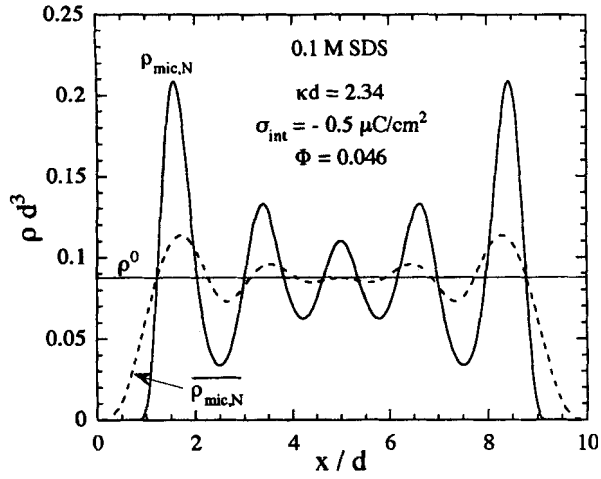

Figure 3. Calculated micelle number density distribution for 0.1-M SDS film of thickness $h/d = 10$.

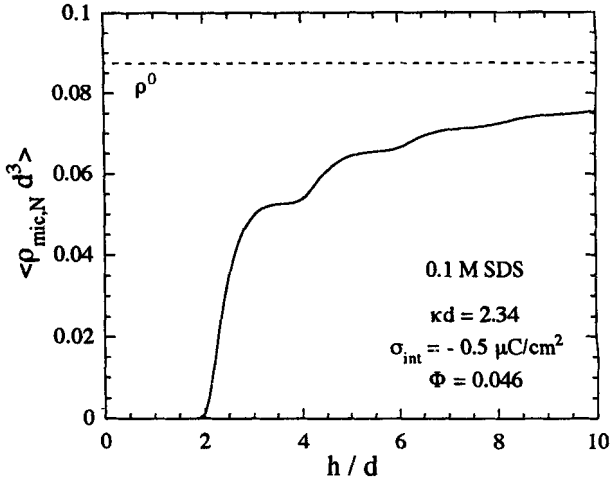

Figure 4. Calculated average micelle number density for 0.1-M SDS film as a function of film thickness.

The same parameters as in Figure 3 apply.

of confined electrostatically stabilized colloids repelled by the interfaces. Confined systems of hard spheres and Lennard-Jones particles show starkly different behavior, with the average density oscillating about the corresponding bulk value (Bitsanis et al., 1988).

Micellar profiles at a series of thicknesses are required to construct the micellar portion of the disjoining pressure isotherm, given in Figure 5. In this 0.1 M-SDS case, the DLVO disjoining pressure term only contributes for $h/d < 2$ and has not been added. The micellar isotherm shows four branches, where a branch denotes a thermodynamically metastable thickness regime with negative slope in Π. The distance between the branches scales with the effective micelle diameter, as the profiles do. Note that the calculated profiles also show unstable regions that cannot be captured experimentally. Further, the calculated disjoining pressures predict the correct trends with increasing surfactant and electrolyte concentrations, but the magnitudes of predicted pressures are high for liquid–gas interfaces (Bergeron and Radke, 1992). Disjoining pressure values are comparable, though, with those measured for cetyltrimethylammonium bromide (CTAB) micelles in the surface forces apparatus (SFA) (Richetti and Kékicheff, 1992). Quantitative agreement with the SFA data, which more closely matches our model assumptions, supports the spherical, monodisperse micelle picture of the confined fluid, while highlighting the need for a more accurate description of foam–film interfaces.

We use the same DFT Tarazona smoothed densities to evaluate the local shear viscosity, although we realize that the hydrodynamic interactions need not have the same range as the excluded volume interactions described by the Tarazona model. Bitsanis et al. (1988) suggest an average about a sphere centered at r of radius equal to the particle diameter for the smoothed density. Comparison of these two smoothing recipes for the local viscosity is given in the Results section.

Local Average Density Model

Following Bitsanis et al. (1987, 1988), we express position-dependent viscosities in micellar films in terms of the viscosities of a hypothetical isotropic fluid at specific values of the smoothed density:

$$\eta(r) = \eta_h[\,\bar{\rho}(r)], \tag{4}$$

where $\eta(r)$ is the local shear viscosity, and $\eta_h(\rho)$ is the viscosity of the corresponding homogeneous fluid at constant density ρ. Thus, at a particular location in the inhomogeneous fluid, the local viscosity is obtained by first computing a weighted average of the varying density about this point and then inputting this smoothed density into an equation that relates the viscosity of an isotropic fluid to the fluid density. This local viscosity, when incorporated into the appropriate differential momentum balances, results in an effective viscosity η^{eff} for the entire film as a function of film thickness h. Since it depends on the flow geometry and boundary con-

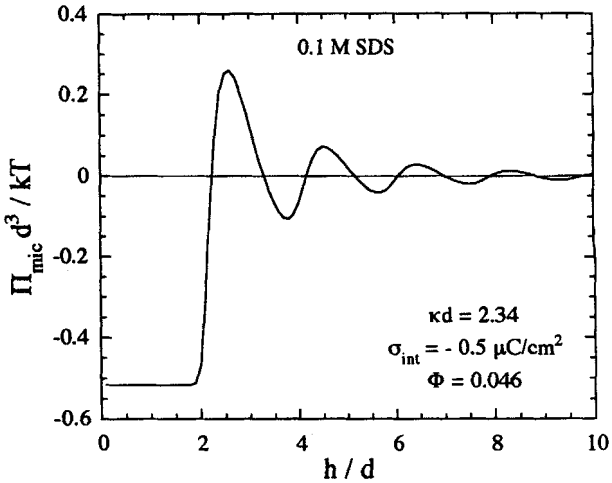

Figure 5. Calculated micellar disjoining pressure isotherm for 0.1-M SDS film as a function of film thickness.

Π_{mic} exhibits four metastable branches. The same parameters as in Figure 3 were used.

ditions, in addition to structuring of the fluid, η^{eff} is not a material property.

Two additional and substantial premises underlie LADM. The first is that the hydrodynamic stresses produced in the system are related to the corresponding velocity gradients through Newtonian constitutive relations, where the proportionality factor is the local shear viscosity, $\eta(r)$, just introduced. The second premise is that during drainage, local thermodynamic equilibrium is maintained in the film. That is, drainage flow does not distort the equilibrium micelle density distributions. Ample discussion of the necessity and justification of these premises for a tractable model is presented by Bitsanis et al. (1988) for noncontinuum molecular fluids.

Film-Drainage Squeeze-Flow Analysis for Effective Viscosities

Visual inspection of soap films in reflected light indicates that films first dimple during drainage (Ivanov and Dimitrov, 1988). Later during drainage and with careful control, however, stable films thin in a plane-parallel manner. We presume plane-parallel thinning in all that follows, with the interfaces rigidified by the adsorption of surfactant, rendering them tangentially immobile. In the model, fluid is squeezed out radially from between two parallel, circular disks whose separation at time t is $h(t)$. The plates or film interfaces are represented by no-slip boundary conditions; the upper interface moves at velocity dh/dt toward the lower one located at $x = 0$. For the thin liquid films of interest, Reynolds' numbers are very low $O(10^{-11})$, permitting use of the creeping-flow limit of the Navier–Stokes equations. This condition also justifies the pseudo-steady-state assumption that the flow at any time t can be treated as steady and that the equilibrium distribution of micelles in the film is not distorted by drainage.

In the inhomogeneous analysis applied to micellar films, position-dependent densities and corresponding variable viscosities are incorporated into the mass and momentum balances, respectively. Here we summarize the salient features of the micellar analysis before proceeding to the results of Bitsanis et al. (1988) for the squeeze-flow effective viscosity. First note that the mass density appearing in the continuity and Navier–Stokes equations is the total mass density, including both micelles and solvent:

$$\rho(x,t;h) = \rho_{\text{mic}}(x,t;h) + \rho_{\text{H}_2\text{O}}(x,t;h), \tag{5}$$

where $\rho(x,t;h)$ is the total mass density, $\rho_{\text{mic}} = (MW_{\text{mic}}/N_A)\rho_{\text{mic, N}}$ is the micelle mass density, and $\rho_{\text{H}_2\text{O}}$ is the aqueous solvent mass density, all local. MW_{mic} is the micelle molecular weight, and N_A is Avogadro's number. We also presume that there is no change in volume upon mixing the micelles and water. This assumption allows us to write the total mass density as

$$\rho(x,t;h) = \frac{1}{\hat{v}_{\text{H}_2\text{O}}}\left[1 - \rho_{\text{mic}}(x,t;h)(\hat{v}_{\text{mic}} - \hat{v}_{\text{H}_2\text{O}})\right], \tag{6}$$

where $\hat{v}_{\text{mic}}$ and $\hat{v}_{\text{H}_2\text{O}}$ are the constant micelle- and water phase-specific volumes. The micelle-specific volume can be estimated by assuming a closest-packed BCC configuration of the spherical micelles:

$$\hat{v}_{\text{mic}} = \frac{\left(\frac{4}{3}\right)^{3/2} d^3 N_A}{2\,MW_{\text{mic}}}. \tag{7}$$

For typical SDS micelles we calculate a specific volume of 2.54×10^{-3} m^3/kg. Other methods of estimating $\hat{v}_{\text{mic}}$ do not appreciably alter the results.

Because film drainage is slow, we assume that the arrangement of the micellar fluid in the film for a given $h(t)$ is that at equilibrium. Thus, we employ our DFT-calculated equilibrium micellar profiles $\rho_{\text{mic,N}}(x;h)$ for $\rho_{\text{mic,N}}(x,t;h)$ in Eq. 6. Note that as $\hat{v}_{\text{mic}}$ for SDS micelles is greater than $\hat{v}_{\text{H}_2\text{O}}$, Eq. 6 shows that positions in the film with relatively high micelle number densities actually have reduced total mass densities. Regions with no micelles, near the interfaces, thus have the highest $\rho(x;h)$, equal to the density of bulk water. Referring to Figure 3, the total mass density distribution through the film resembles an upside-down micelle profile: peaks in the micelle profile denote minima in $\rho(x;h)$, whereas troughs in the micelle distribution denote local maxima in $\rho(x;h)$. Conversely, if colloidal particles denser than the solvent ($\hat{v}_{\text{mic}} < \hat{v}_{\text{H}_2\text{O}}$) are considered, then regions of high particle density increase the corresponding total mass density. Both cases are explored in the Results section. The total mass density is incorporated into the continuity equation, with the quasi-steady-state approximation, and no-slip boundary and symmetry conditions.

The hydrodynamic stresses in the momentum balances are related to the velocity and viscosity profiles through Newtonian constitutive relations, which in turn demand expressions for the shear viscosity, η_h, of homogeneous colloidal fluids. These usually take the form of power series in the particle volume fraction Φ (Batchelor and Green, 1972; Russel, 1980; Sherwood, 1980). The series coefficients are functions of particle size, the static double-layer characteristics about the particles, the surface charge or potential on the particles, and particle polarizabilities. The simplest form of the shear viscosity is the Stokes–Einstein relation (Einstein, 1956), obtained by truncating terms higher than first order in the series. This equation is accurate for dilute hard-sphere suspensions. It becomes progressively worse for volume fractions approaching the fluid–solid phase transition ($\Phi \sim 0.55$). Because the micellar fluids of interest represent micelle volume fractions of 5% to 10%, even locally in the film, we use the Stokes–Einstein relation:

$$\frac{\eta(x)}{\eta^0} = \frac{\eta_h[\overline{\rho_{\text{mic,N}}}(x)]}{\eta^0} = 1 + \frac{5\pi}{12}\overline{\rho_{\text{mic,N}}}(x)d^3, \tag{8}$$

where η^0 is the solvent viscosity. This relation, in conjunction with the DFT coarse-grained number densities $\overline{\rho_{\text{mic,N}}}(x)$, determines the local viscosity (profiles) that relate the Newtonian stresses to the velocity profiles through the film.

Integration of the momentum balances yields an expression for the hydrodynamic pressure. Comparison with the corresponding relation for the pressure in the homogeneous

case allows definition of an equivalent or effective viscosity for an inhomogeneous colloidal fluid undergoing squeeze flow between parallel disks (Bitsanis et al., 1988):

$$\eta^{\text{eff}}(h) = \frac{\frac{h^3}{12}\left[\langle \rho(x;h)\rangle + h\frac{\partial\langle \rho(x;h)\rangle}{\partial h}\right]}{\int_0^h d\zeta\rho(\zeta)\int_0^\zeta d\vartheta\frac{h-2\vartheta}{2\eta(\vartheta)}}, \qquad (9)$$

where $\langle \rho(x;h)\rangle$ is the average total density through the film of thickness h. Recall that $\rho(x)$ is the total mass density, including micelles and solvent, given by Eq. 5, and that $\eta(x)$ is the local viscosity, given by Eq. 8, which depends on the micellar profiles calculated with density functional theory. Equation 9 applies to any confined particulate system, with or without a suspending solvent, that satisfies the LADM assumptions (Laso, 1993). In the limiting case of no micelles in the film, $\rho(x;h) = \rho_{H_2O} = 1/\hat{v}_{H_2O}$, allowing analytic solution of Eq. 9, which yields the desired result that $\eta^{\text{eff}}(h) = \eta^0$. In inhomogeneous systems, the derivative term in the numerator of Eq. 9 plays a key role. Recall in Figure 4 for 0.1-M SDS, the average number density of micelles, $\langle \rho_{\text{mic,N}}(x;h)\rangle$, is an increasing function of thickness. Thus, the average mass density in the film, $\langle \rho(x;h)\rangle$, is a decreasing function, the derivative being negative. Systems with other interparticle interactions or different $\hat{v}_{\text{mic}}$ can have positive derivatives and correspondingly different behavior. By integrating the stress over the upper disk surface to yield the force on the moving plate, we obtain formally the inhomogeneous analogue of the Stefan–Reynolds' thinning equation (Stefan, 1874; Reynolds, 1886):

$$\frac{dh}{dt} = -\frac{2h^3}{3\pi R^2}\frac{[P_c - \Pi(h)]}{\eta^{\text{eff}}(h)}, \qquad (10)$$

where both the effective viscosity and the disjoining pressure rely on the equilibrium micellar distributions through the film. Details of the calculation are available elsewhere (Laso, 1993).

Effective Viscosities and Thinning Curves

The solid line in Figure 6 shows the calculated effective viscosity as a function of film thickness corresponding to the micelle profile and disjoining pressure displayed in Figures 3 and 5, respectively. For this case, the homogeneous micellar fluid viscosity η_h ($\rho^0_{\text{mic,N}}$) from the Stokes–Einstein relation is 1.11 η^0, using Eq. 8 evaluated at the bulk micelle number density. The dash-dot line corresponds to an average viscosity of the film, $\eta_{\text{av}}(h) = \eta(\langle \rho_{\text{mic,N}}(x;h)\rangle)$, calculated using the Stokes–Einstein relation in Eq. 8, but evaluated at the average micelle density for a given film thickness presented in Figure 4. Note first that both $\eta^{\text{eff}}(h)$ and $\eta_{\text{av}}(h)$ are always less than $\eta(\rho^0_{\text{mic,N}})$, differing by less than 10% from the bulk micellar solution shear viscosity for all h, but approaching this homogeneous value at larger film thicknesses. Additionally, $\eta^{\text{eff}}(h)$ is always less than $\eta_{\text{av}}(h)$, and $\eta^{\text{eff}}(h)$ shows more structure, particularly for thinner films. As the film thins, the effective viscosity follows a decreasing trend, reaching the limiting value of η^0 when all micelles have been completely expelled from the film at $h/d < 2$. Because the aqueous solvent is treated as a continuum, we do not gain any information about the effective viscosity in very thin, Newton black films where the hydrodynamic analysis may break down.

These general characteristics of micellar film effective viscosities can be explained by considering the behavior of the underlying micelle distributions, the relative densities of micelles and solvent, and the squeeze-flow velocity profiles. As expressed in Eq. 9, the effective viscosity is an averaged quantity depending strongly on the corresponding average micelle density and not on the details of the structured profiles. From Figure 4, the average micelle number density decreases as the film thins due to the electrostatic repulsions between the micelles, and $\langle \rho_{\text{mic,N}}(x;h)\rangle$ is always less than the bulk density for the conditions chosen. This yields the surprising result that the effective viscosity is never higher than that of the corresponding bulk solution, and actually decreases for thinner films. This result is opposite of that predicted for Lennard-Jones fluids where the attractive potentials can lead to viscosities several times that of the bulk fluid (Bitsanis et al., 1987, 1988).

The effective viscosity is additionally lower than $\eta_{\text{av}}(h)$, because $\eta^{\text{eff}}(h)$ relies on values of the local (Stokes–Einstein) viscosity evaluated at the smoothed density, which is defined to exhibit less pronounced structure than the actual density profile (cf. Figure 3). It is interesting that despite the dependence of $\eta^{\text{eff}}(h)$ on the smoothed density, it shows more oscillations than $\eta_{\text{av}}(h)$, which depends on the average of the full number density profile. To understand this behavior we must consider independently the effects of varying total mass density and local viscosity with film thickness. This is accomplished by calculating $\eta^{\text{eff}}(h)$ in the model case where the micelle and water-specific volumes are the same ($\hat{v}_{\text{mic}} = \hat{v}_{H_2O} = 1\times10^{-3}$ m^3/kg) with the local viscosity given by Eq. 8, and

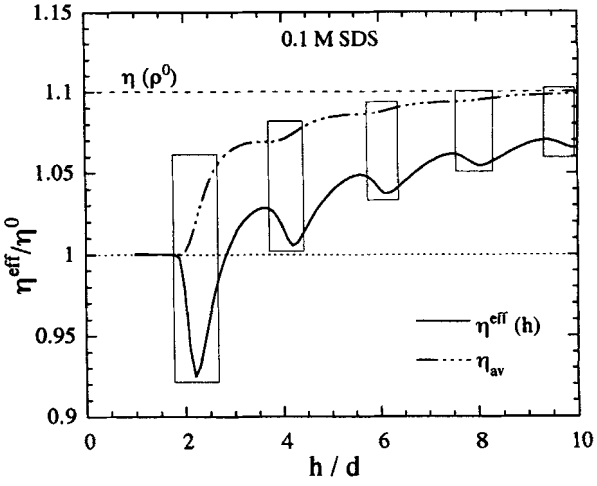

Figure 6. Calculated effective viscosity for a 0.1-M SDS micellar film as a function of film thickness.

The solid line represents the effective viscosity calculated from Eq. 9 using either the Tarazona or Bitsanis coarse-grained density recipes that superimpose. The dash-dot line corresponds to the viscosity calculated from Stokes–Einstein relation, Eq. 8 using the average micelle number density in the film as a function of thickness, in Figure 4. The boxes represent thickness regimes where the film is unstable, as evident from positive disjoining pressure slopes in Figure 5.

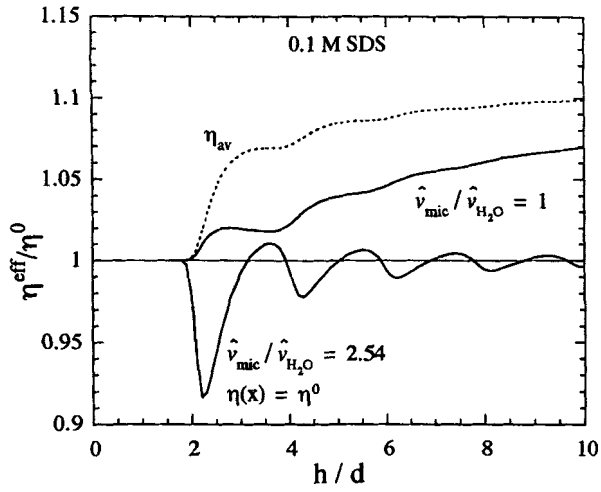

Figure 7. Effects of varying local viscosity and mass density on the effective viscosity of a 0.1-M SDS micellar film,

The dotted line corresponds to the viscosity calculated from Stokes-Einstein relation, using the average micelle number density in the film as a function of thickness, in Figure 4.

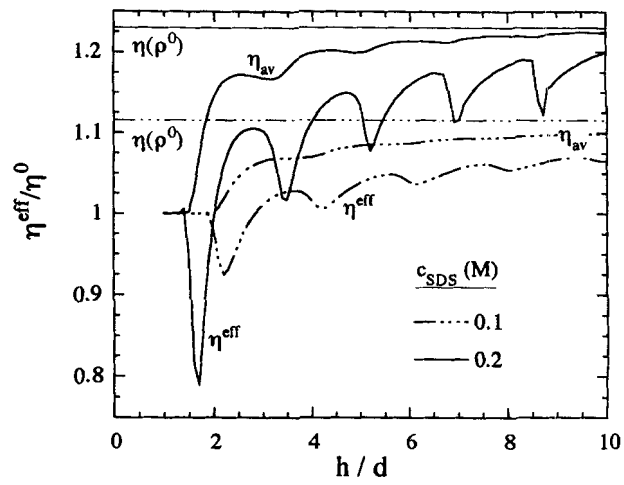

Figure 8. Comparison of calculated effective viscosities for two surfactant concentrations.

the case where the specific volumes are different ($\hat{v}_{mic} = 2.54 \times 10^{-3}$ m^3/kg; $\hat{v}_{H_2O} = 10^{-3}$ m^3/kg) but the local viscosity is set equal to the solvent viscosity ($\eta(x) = \eta^0$). These model cases are presented in Figure 7 together with $\eta_{av}(h)$. We see that the full effective viscosity in Figure 6 is a combination of the two cases described earlier, with the varying density giving rise to the structural character of $\eta^{eff}(h)$. The effect of the Stokes–Einstein viscosity for these dilute systems is not pronounced. It bears noting that in this micellar case the two smoothing recipes of Bitsanis et al. (1988) and Tarazona (1985) mentioned earlier yield indistinguishable effective viscosities.

The boxed regions labeled in Figure 6 correspond to thicknesses where the slope of the disjoining pressure is positive. In these regions, the interior layer of micelles is expelled from the film, producing a rearrangement of the remaining micellar layers in the film. The box at $h/d \sim 10$ represents the transition from five micellar layers to four; the box at $h/d \sim 2$ depicts the expulsion of the last micelle layer. Recall that at these thicknesses where $d\Pi/dh > 0$ the film is thermodynamically unstable; thus the micellar profiles generated for these thicknesses do not represent realizable equilibrium profiles. Hence, calculated effective viscosities for these unstable thicknesses are likely unreliable, as the film does not thin in a plane-parallel manner through these regions. Rather, rapid hole-sheeting instabilities commence (Jiménez-Laguna, 1991; Bergeron et al., 1992).

Even in the stable regions, the model displays nonintuitive results for the film effective viscosity as evident for $h \sim 2.5\,d$ in Figure 6 where $\eta^{eff}(h)/\eta^0$ falls below unity. As the film thins through this region, the average micelle density first increases sharply (a single number density peak rises and narrows), resulting in large (negative) derivative term in Eq. 9 that lowers the value of $\eta^{eff}(h)$. Subsequent expulsion of the last micelle layer decays the derivative term, with the effective viscosity approaching that of the solvent. Examination of the velocity profiles (Laso, 1993) demonstrates that effective viscosities less than η^0 simply imply that the structuring of less dense micelles causes micellar films to thin faster than a homogeneous water film at these thicknesses, this despite the local viscosity, which is higher in regions of higher micelle densities. Within the effective viscosity model, the presence of less dense micelles enhances film thinning rates.

Figure 8 compares 0.1-M ($\Phi = 0.046$) and 0.2-M ($\Phi = 0.092$) effective viscosities and their corresponding $\eta_{av}(h)$ viscosities. The 0.2-M SDS η^{eff} exhibits considerably more structure than the 0.1-M case, commensurate with the calculated micellar profiles. Again, η^{eff} is always less than η_{av}, and $\eta^{eff} < \eta^0$ for small (unstable) thicknesses indicative of faster thinning films, as described earlier. The important result is that the pronounced micellar structure in the films, arising from repulsive electrostatic micelle–micelle interactions, produces effective film viscosities that are always lower (by less than 10%) than the bulk micellar solution shear viscosity and that effective viscosities decrease at smaller film thicknesses.

Figure 9 compares the effective film viscosities of fluids with different particle-to-solvent-specific volumes, but having the same underlying repulsive interactions as 0.1-M SDS micelles depicted in Figures 3–5. Recall that the 0.1-M SDS case represents particles of lower bulk mass density than the suspending solvent, with $\hat{v}_{H_2O}/\hat{v}_{mic} = 1/2.54$. In Figure 9 the particles are five times denser than the solvent ($\hat{v}_{mic} = 5 \times 10^{-4}$ m^3/kg). The effective viscosity in this case ($\hat{v}_{mic} < \hat{v}_{H_2O}$) is almost a mirror image of the 0.1-M SDS $\eta^{eff}(h)$, also with values below the averaged viscosity, except at the smallest thicknesses where η^{eff} rises to $\sim 1.14\ \eta^0$. The reflection of $\eta^{eff}(h)$ results from the increased mass density of the particle phase relative to the solvent. Again, $\eta^{eff}(h)$ is lower than η^0 and $\eta_{av}(h)$ for most thicknesses because the interparticle repulsions keep the mean particle density in the film lower than in the bulk, and because η^{eff} relies on the smoothed densities rather than the full number density profile. The large peak at $h/d \sim 2$ reflects the analogous behavior of the $h\partial\langle \rho(x;h)\rangle/\partial h$ term in Eq. 9 described earlier for SDS films.

When the ratio $\hat{v}_{H_2O}/\hat{v}_{mic}$ is raised above about 10, the effective viscosity shows large, decaying oscillations with film thickness not unlike those predicted for Lennard-Jones molecules in a vacuum (Bitsanis et al., 1988), where the cor-

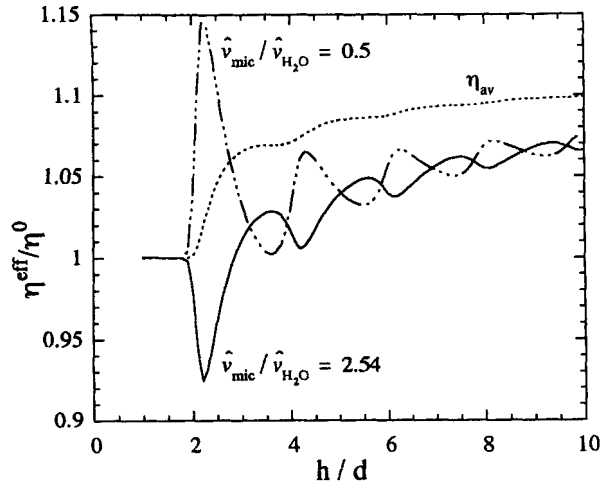

Figure 9. Comparison of calculated effective viscosities for two micelle (colloid) specific volumes.

The dash-dot line represents much denser material, ~ five times the density of SDS micelles, with $\hat{v}_{mic} = 5 \times 10^{-4}$ m^3/kg. The 0.1-M SDS density profiles in Figures 3 and 4 were used for both cases, thus presuming the colloid particles to interact as SDS micelles.

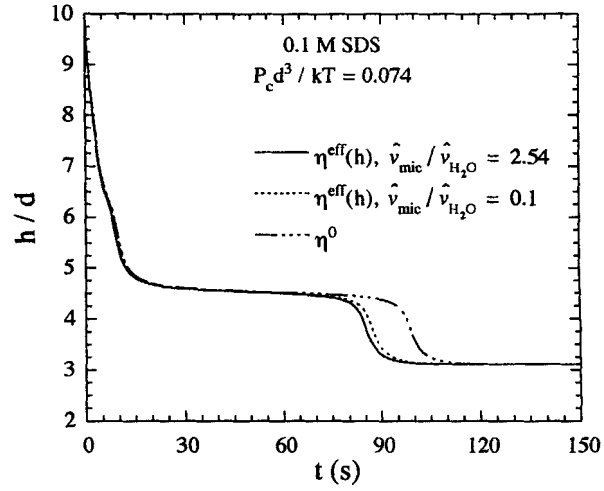

Figure 10. Comparison of calculated thinning curves for an 0.1-M SDS foam film using various effective viscosities.

The film is subject to an imposed capillary pressure just above the second maximum in the disjoining pressure in Figure 5.

responding particle-to-solvent density ratio is infinite. Solution volume fractions of even 10% can produce significant equilibrium ordering within thin liquid films because ionic micelles exhibit large effective sizes that arise from their Debye atmospheres. Film-drainage resistance at the same solution volume fractions, however, is not significantly enhanced since viscous forces reflect the actual micelle hard-sphere diameter.

In Figure 10 we show calculated film thinning curves obtained by integrating Eq. 10, using our self-consistent disjoining pressures and effective viscosities. Here the capillary pressure has been set to 0.074 d^3/kT, slightly higher than the second maximum at $h/d = 4$ in Π_{mic} (see Figure 5). As in Figure 1, we see that the thinning is nonmonotonic and qualitatively very similar to what is observed experimentally (Nikolov and Wasan, 1989; Bergeron and Radke, 1992; Sonin and Langevin, 1993; Krichevksy and Stavans, 1995) in the number of steps, their relative duration, and the thicknesses at which they occur. A quantitative comparison with experiment is not possible because of the overestimation of the disjoining pressures (Pollard and Radke, 1994). The extended steplike regions in the curve represent thicknesses where the driving force for thinning, the difference between P_c and Π, is relatively small, namely at the local maxima in $\Pi(h)$. The transitions between steps correspond to large driving forces, where the film passes over the local maximum in the disjoining pressure into unstable regions that dip into the attractive region as the interior layer of micelles is expelled from the film. The three curves in Figure 10 denote results for the two effective viscosities with $\hat{v}_{mic} = 2.54 \times 10^{-3}$ m^3/kg and 10^{-4} m^3/kg and for the solvent viscosity $\eta^0 = 1$ mPa·s. Note that except in the transition region for $4.5 > h/d > 3$, the curves are almost superimposable. In this last transition, the film with the very dense particles ($\hat{v}_{mic} = 10^{-4}$ m^3/kg) thins the slowest. The SDS micellar film thinning is quite close to the water viscosity result, clearly demonstrating that micelles, although structured within the film, do not contribute appreciably to the viscous resistance of the film. Our ability to capture the same effects observed experimentally indicates that the driving force for the stepwise thinning is the oscillatory disjoining pressure, not anomalous viscosity effects of the micellar fluid in the film. Use of the homogeneous micellar solution viscosity is quite adequate for descriptions of the dynamics of ionic micellar films.

Conclusions

We have extended the LADM of Bitsanis et al. (1987) for squeeze-flow effective viscosities of molecular fluids (Bitsanis et al., 1988) to ionic micellar films, incorporating the solvent appropriately into the hydrodynamic analysis. We employ our previously presented DFT micellar profiles and disjoining pressures (Pollard and Radke, 1994), also using Tarazona smoothing (Tarazona, 1985) for the local shear viscosities. A simple Stokes–Einstein relation relates the coarse-grained density to the shear viscosity; it is adequate for the low micellar volume fractions of interest. Calculated micellar film effective viscosities are generally less than that of the bulk micellar solution due to the electrostatic repulsions between the charged micelles. For these dilute systems, the effect of the densities of the particle and solvent phases plays a more important role than the Stokes–Einstein local viscosities. The model displays initially nonintuitive results of effective viscosities less than the solvent viscosity, at very small film thicknesses, that indicate faster thinning of micellar films relative to homogeneous aqueous films. Calculated thinning curves closely resemble experimental observations in the stepwise thinning behavior, displaying decreasing slopes and increased step durations at later times.

The main conclusion of the calculation is that although ionic micelles are predicted to structure within the film from our DFT model, micellar layering does not lead to a significant change in the film's viscous resistance. This conclusion is consistent with ESR data (Povich and Mann, 1973) and

light-scattering measurements (Krichevsky and Stavans, 1995) of ionic micellar films, as well as surface forces viscosity measurements for pure fluids (Israelachvili, 1986). We have thus successfully linked our DFT-calculated micellar profiles and disjoining pressures with continuum hydrodynamic analyses for hole formation, expansion, and film drainage (Bergeron et al., 1992).

Acknowledgments

This work was partially supported by the Assistant Secretary for Fossil Energy, Office of Oil, Gas, and Shale Technologies of the U.S. Department of Energy under Contract DE-AC03-76SF00098 to the Lawrence Berkeley Laboratory of the University of California. One of the authors (M.L.P.) acknowledges a Henkel Corporation of America ACS Colloid Division Graduate Research Fellowship.

Notation

r = general coordinate variable, m
R = disk radius, m
x = position normal to the film interfaces measured from one of the interfaces, m
$\Pi_{DLVO}(h)$ = DLVO wall–wall contribution to the disjoining pressure, Pa
$\Pi_{mic}(h)$ = micellar contribution to the disjoining pressure, Pa
ρ = bulk mass or number density, kg/m^3 or m^{-3}
$\bar{\rho}(r)$ = smoothed or coarse-grained number density distribution, m^{-3}

Literature Cited

Batchelor, G. K., and J. T. Green, "The Determination of the Bulk Stress in a Suspension of Spherical Particles to Order c^2," *J. Fluid Mech.*, **56**, 401 (1972).

Bergeron, V., "Forces and Structure in Surfactant-Laden, Thin-Liquid Films," PhD Thesis, Univ. of California, Berkeley (1993).

Bergeron, V., A. I. Jiménez-Laguna, and C. J. Radke, "Hole Formation and Sheeting in the Drainage of Thin Liquid Films," *Langmuir*, **8**, 3027 (1992).

Bergeron, V., and C. J. Radke, "Equilibrium Measurements of Oscillatory Disjoining Pressures in Aqueous Foam Films," *Langmuir*, **8**, 3020 (1992).

Bergeron, V., and C. J. Radke, "Disjoining Pressure and Stratification in Asymmetric Thin-Liquid Films," *Coll. Poly. Sci.*, **273**, 165 (1995).

Bitsanis, I., J. J. Magda, M. Tirrell, and H. T. Davis, "Molecular Dynamics of Flow in Micropores," *J. Chem. Phys.*, **87**, 1733 (1987).

Bitsanis, I., T. K. Vanderlick, M. Tirrell, and H. T. Davis, "A Tractable Molecular Theory of Flow in Strongly Inhomogeneous Fluids," *J. Chem. Phys.*, **89**, 3152 (1988).

Derjaguin, B. V., and L. Landau, "Theory of the Stability of Strongly Charged Lyophobic Sols and of the Adhesion of Strongly Charged Particles in Solutions of Electrolytes," *Acta Physicochim. URSS*, **14**, 633 (1941).

Einstein, A., *Investigation on the Theory of the Brownian Movement*, Dover, New York (1956).

Exerowa, D., T. Kolarov, and K. Khristov, "Direct Measurement of Disjoining Pressure in Black Foam Films. I. Films from an Ionic Surfactant," *Coll. Surf.*, **22**, 171 (1987).

Israelachvili, J. N., "Measurement of the Viscosity of Liquids in Very Thin Films," *J. Coll. Int. Sci.*, **110**, 263 (1986).

Ivanov, I. B., and D. S. Dimitrov, "Thin Film Drainage," *Thin Liquid Films*, I. B. Ivanov, ed., Marcel Dekker, New York, p. 379 (1988).

Jiménez-Laguna, A. I., "Stability of Thin Liquid Films: Theory and Application to Foam Flow in Porous Media," PhD Thesis, Univ. of California, Berkeley (1991).

Johonnott, E. S., "Thickness of Black Spots in Thin Liquid Films," *Philos. Mag.*, **47**, 501 (1899).

Krichevsky, O., and J. Stavans, "Micellar Stratification in Soap Films —A Light Scattering Study," *Phys. Rev. Lett.*, **74**, 2752 (1995).

Laso, M., "Modeling of Structure and Forces in Thin Micellar Liquid Films," PhD Thesis, Univ. of California, Berkeley, (1993).

Mysels, K. J., and M. N. Jones, "Direct Measurement of the Variation of Double-Layer Repulsion with Distance," *Discuss. Farad. Soc.*, **42**, 42 (1966).

Nikolov, A. D., P. A. Kralchevsky, I. B. Ivanov, and D. T. Wasan, "Ordered Micelle Structuring in Thin Films Formed from Anionic Surfactant Solutions. II. Model Development," *J. Coll. Int. Sci.*, **133**, 13 (1989).

Nikolov, A. D., and D. T. Wasan, "Ordered Micelle Struturing in Thin Films Formed from Anionic Surfactant Solutions. I. Experimental," *J. Coll. Int. Sci.*, **133**, 1 (1989).

Nikolov, A. D., and D. T. Wasan, "Dispersion Stability Due to Structural Contributions to the Particle Interaction as Probed by Thin Liquid Film Dynamics," *Langmuir*, **8**, 2985 (1992).

Nikolov, A. D., D. T. Wasan, N. D. Denkov, P. A. Kralchevksy, and I. B. Ivanov, "Drainage of Foam Films in the Presence of Nonionic Micelles," *Prog. Coll. Poly. Sci.*, **82**, 87 (1990).

Overbeek, J. T. G., "The Interaction between Colloidal Particles," *Colloid Science*, H. R. Kruyt, ed., Elsevier, New York, p. 245 (1952).

Perrin, J., "La Stratification des Lames Liquides," *Ann. Phys.*, **9**, 160 (1918).

Pollard, M. L., and C. J. Radke, "Density-Functional Modeling of Structure and Forces in Thin Micellar Liquid Films," *J. Chem. Phys.*, **101**, 6979 (1994).

Povich, M. J., and J. A. Mann, "Physical Properties of Thin Soap Films Measured by Electron Spin Resonance Exchange Broadening," *J. Phys. Chem.*, **77**, 3020 (1973).

Reynolds, O., "On the Theory of Lubrication," *R. Soc. London: Philos. Trans.*, **177**, 157 (1886).

Richetti, P., and P. Kékicheff, "Direct Measurement of Depletion and Structural Forces in a Micellar System," *Phys. Rev. Lett.*, **68**, 1951 (1992).

Russel, W. B., "Review of the Role of Colloidal Forces in the Rheology of Suspensions," *J. Rheol.*, **24**, 287 (1980).

Sherwood, J. D., "The Primary Electroviscous Effect in a Suspension of Spheres," *J. Fluid Mech.*, **101**, 609 (1980).

Sonin, A. A., and D. Langevin, "Stratification Dynamics of Thin Films Made from Aqueous Micellar Solutions," *Europhys. Lett.*, **22**, 271 (1993).

Stefan, J., "Vershche uber die Scheinbare Adhasion," *Sitzungsber Math.-Naturwiss. Akad. Wiss. Wein.*, **1**, 713 (1874).

Tarazona, P., "Free-Energy Density Functional for Hard Spheres," *Phys. Rev. A*, **31**, 2672 (1985).

Vanderlick, T. K., L. E. Scriven, and H. T. Davis, "Molecular Theories of Confined Fluids," *J. Chem. Phys.*, **90**, 2422 (1989).

Vrij, A., "Possible Mechanism for the Spontaneous Rupture of Thin, Free Liquid Films," *Discuss. Farad. Soc.*, **42**, 23 (1966).

Wasan, D. T., A. D. Nikolov, P. A. Kralchevsky, and I. B. Ivanov, "Universality in Film Stratification Due to Colloid Crystal Formation," *Coll. Surf.*, **67**, 139 (1992).

Manuscript received Aug. 14, 1995, and revision received Feb. 9, 1996.